Inorganic Chemistry

Article

pubs.acs.org/IC

New Antiferromagnetic Perovskite $CaCo_3V_4O_{12}$ Prepared at High-Pressure and High-Temperature Conditions

Sergey V. Ovsyannikov,*[,†,‡] Yury G. Zainulin,[†] Nadezda I. Kadyrova,[†] Alexander P. Tyutyunnik,[†] Anna S. Semenova,[†] Deepa Kasinathan,[§] Alexander A. Tsirlin,[⊥] Nobuyoshi Miyajima,[‡] and Alexander E. Karkin[∥†]

[†]Institute for Solid State Chemistry, Russian Academy of Sciences, Urals Division, 91 Pervomayskaya Strasse, Yekaterinburg 620990, Russia

[‡]Bayerisches Geoinstitut, Universität Bayreuth, Universitätsstrasse 30, Bayreuth D-95447, Germany

[∥]Institute of Metal Physics, Russian Academy of Sciences, Urals Division, GSP-170, 18 S. Kovalevskaya Strasse, Yekaterinburg 620990, Russia

[§]Max Planck Institute for Chemical Physics of Solids, Nöthnitzer Strasse 40, 01187 Dresden, Germany

[⊥]National Institute of Chemical Physics and Biophysics, Akadeemia tee 23, 12618 Tallinn, Estonia

Supporting Information

ABSTRACT: A new perovskite, $CaCo^{2+}{}_3V^{4+}{}_4O_{12}$, has been synthesized at high-pressure and high-temperature (HP-HT) conditions. The properties of this perovskite were examined by a range of techniques. $CaCo_3V_4O_{12}$ was found to adopt a double-perovskite cubic lattice [a = 7.3428(6) Å] with $Im\bar{3}$ symmetry. We have established that this new perovskite is stable at ambient conditions, and its oxidation and/or decomposition at ambient pressure begins above 500 °C. It undergoes an abrupt antiferromagnetic transition around 98 K. Electrical resistivity data suggest semimetallic conductivity in the temperature range of 1.6−370 K. We have established that the Co^{2+} ions in $CaCo_3V_4O_{12}$ are in the high-spin state with a sizable orbital moment, even though their square-planar oxygen coordination could be more suitable for the low-spin state, which is prone to Jahn−Teller distortion. Electrical resistivity curves also exhibit a distinct steplike feature around 100 K. $CaCo_3V_4O_{12}$ is a first example of perovskite in which the sites A′ are fully occupied by Co^{2+} ions, and hence its synthesis opens the door to a new class of double perovskites, $ACo_3B_4O_{12}$, that may be derived by chemical substitution of the A sublattice by lanthanides, sodium, strontium, and bismuth and by other elements and/or of the B sublattice by some other transition metals.

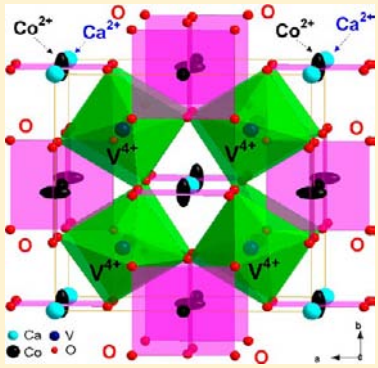

INTRODUCTION

Perovskites, with the general formula ABO_3 (where A = alkali, alkali-earth, rare-earth, Pb, and Bi and B = transition metals, Ga, Ge, Sb, and Sn), are a very common class of oxide materials that find applications in a wide range of technologies. They demonstrate plenty of exciting phenomena and properties, e.g., ferroelectricity, resistive switching (insulator−metal transitions), colossal magnetoresistance, colossal dielectric constants, and others.[1,2] A perovskite structure has two types of cation sites: octahedrally coordinated B sites and A sites with variable coordination number. In the overwhelming majority of perovskites, the cations that occupy the B sites interact through the B−O−B network and determine electronic properties, whereas those at the A sites normally remain electronically inactive but can tune both the oxidation states of B cations and the geometry of their octahedra. Chemical and structural modifications of perovskites lead to new possibilities for their applications. Nowadays, more complex materials with the perovskite-based structure are being designed and investigated.[3,4] For example, the structures of so-called "double perovskites" are based on the perovskite unit(s) but additionally feature cation ordering at the B sites (e.g., materials like $A_2BB'O_6$ and $A'ABB'O_6$)[5−7] and/or at the A sites (e.g., materials like $AA'_3B_4O_{12}$ and $AA'_3B_2B'_2O_{12}$).[3,8]

Double perovskites with the formula $AA'_3B_4O_{12}$ comprise an additional cation site A′ that has square-planar oxygen coordination. It accommodates small-sized cations of transition metals.[3,8] A close location of the B and A′ sites facilitates electronic interactions through the A′−O−B chains. This can lead to new exciting phenomena, such as, e.g., an isostructural transition in $LaCu_3Fe_4O_{12}$ at low temperatures or high pressures.[9−11] Chemical substitution of cations at the A or B sites in the double-perovskite structure can also lead to remarkable variations in magnetic, electronic, and other properties, e.g., in $CaCu_3B_4O_{12}$ for B = Ti,[12,13] Mn,[14] Ru,[15] V,[16] Fe,[17] Pt,[18] and others. However, square-planar oxygen coordination of the A′ sites hints that this position may be taken only by those ions that are prone to Jahn−Teller distortion.[3,4,19,20] There are numerous examples of double

Received: March 19, 2013
Published: October 1, 2013

   dx.doi.org/10.1021/ic400649h | Inorg. Chem. 2013, 52, 11703−11710

perovskites in which the A′ sites are fully occupied by Cu^{2+} [9−18] and Mn^{3+} ions.[21−25]

High-pressure and high-temperature (HP-HT) synthesis is one of the promising methods for fabrication of new unusual materials. Its application allowed the construction of new perovskite systems, e.g., for a vanadium-based perovskite family, such as $CaCu_3V_4O_{12}$,[16] $(Na,Y)Cu_3V_4O_{12}$,[26] and (Na,Ca,La)-$Mn_3V_4O_{12}$ with variable oxidation states of the Mn and V ions[27] and $CaPd_3(Ti,V)_4O_{12}$.[28] Furthermore, the HP-HT treatment can force other transition-metal ions to take the A′ site or even the A site in the structure. Using this method, new, highly unconventional perovskites with the A′ sites taken by Fe^{2+} ions $(CaFe_3Ti_4O_{12})$[29] and the A sites taken by Mn^{2+} ions $(Mn^{2+}Mn_3^{3+}Mn_4^{3.25+}O_{12})$[30] have been prepared. Moreover, recent studies showed that it is possible to substitute part of the Cu ions in $CaCu_3V_4O_{12}$ by Fe^{3+} [31] or Co^{2+} ions.[32] However, the maximal substitution rate in the above cases is less than $^1/_3$ at synthesis pressures below 8 GPa.

In this work, using a HP-HT technique, we have prepared a new vanadate perovskite, $CaA'_3V_4O_{12}$, in which the A′ sites are fully occupied by Co ions. This is the first example of a double perovskite with the A′ sites fully filled by Co ions. We have established a cubic double-perovskite lattice of this material and investigated its structural, magnetic, and electronic transport properties. We have found that near 100 K this perovskite exhibits an abrupt antiferromagnetic ordering transition accompanied by a steplike feature in the temperature dependence of electrical resistivity. We have determined the oxidation states of the Co and V ions, analyzed the spin state of the Co ions, and discussed the conditions of the formation of the double-perovskite structure.

EXPERIMENTAL SECTION

HP-HT synthesis was accomplished on a 1200 tonne multianvil press at BGI (Bayreuth, Germany). For the synthesis, we used powdery mixtures with purities of better than 99.9% of $Ca(VO_3)_2$, $Co(VO_3)_2$, and Co. To avoid undesirable chemical reactions, the samples were synthesized in a cylindrical capsule made of a 25 μm thin rhenium foil. This rhenium capsule, a $LaCrO_3$ heater, a MgO insulating cylinder, W3Re/W25Re thermocouples, and other components were adjusted in an octahedral container made of $(MgO)_{0.95}(Cr_2O_3)_{0.05}$.[30] Pressure was generated between eight tungsten carbide cubic anvils with truncated corners. A pyrophyllite gasket was employed as a pressure-transmitting medium. Other details of the synthesis were similar to those reported earlier.[33,34] We have synthesized a dozen samples at pressures between 14 and 18 GPa and temperatures between 900 and 1300 °C. Typical times of the syntheses were between 30 min and 8 h. We found that synthesis at 15−16 GPa and temperatures of 1000−1100 °C leads to the formation of bulk polycrystalline samples with minor impurities of $CaVO_3$ perovskite and VO_2-based solid solutions. Prolonged synthesis at a higher pressure of 18 GPa and similar temperatures of 1100−1200 °C led to the formation of relatively big single-crystalline (typically twinned) samples of sizes of ∼20−100 μm. Bulk polycrystalline samples were further selected for powder X-ray diffraction (XRD) and magnetic and electronic transport studies, while single-crystalline samples were used for crystal structure refinement. After recovery to ambient conditions, the $CaCo_3V_4O_{12}$ sample persists indefinitely as a metastable phase.

The morphology and chemical composition of the products were examined by scanning electron microscopy (SEM) and electron microscopy studies using a JEOL-JSM 6390 LA microscope with a JED-2300 attachment (Figures S1−S3 in the Supporting Information, SI). These systematic studies performed on several samples showed that the chemical composition of this perovskite, in general, is close to ideal with a ratio of Ca/Co/V cations of 1.00/3.00/4.00. However, slight deviations from this stoichiometry may be observed in smaller regions of not fully reacted samples. More details on this issue may be found in the SI.

Transmission electron microscopy (TEM) analysis (Figures 1 and 2) was performed using a Philips CM20 FEG (field emission gun) system, equipped with an energy-dispersive X-ray (EDX) analyzer, operated at 200 kV. The selected-area electron diffraction (SAED) patterns at 105 K were taken using a liquid-nitrogen-cooling holder. The TEM foil was prepared at low voltages of 4 kV and an incidence angle of 8° by a conventional Ar-ion milling method.

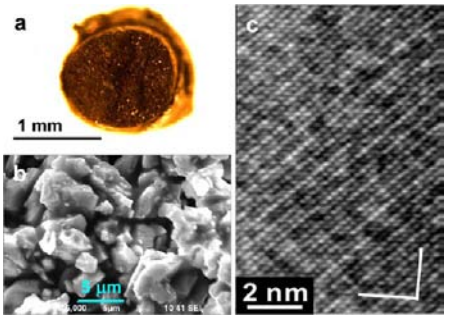

Figure 1. Photograph and microstructure of $CaCo_3V_4O_{12}$. (a) Photograph of the bulk sample: top view of a cylindrical sample; the ragged edges are rests of the rhenium capsule. (b) SEM image of microcrystallites. (c) High-resolution TEM image of the ⟨001⟩ zone axis obtained at ambient temperature. The white axes are the principal axes of a_1 and a_2.

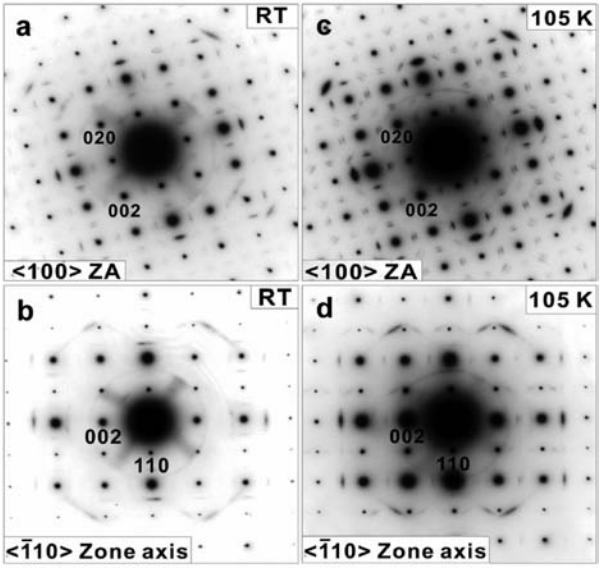

Figure 2. SAED patterns of $CaCo_3V_4O_{12}$ obtained at room temperature, 295 K (a and b), and at 105 K (c and d). The spot reflections unambiguously suggest a cubic symmetry ($Im\bar{3}$ space group). The dashlike reflections (they are seen especially distinctly in the patterns a and c) hint at the possible existence of incommensurate structural modulations in the cubic lattice.

Preliminary structural characterization of the samples synthesized in HP-HT conditions was performed at ambient conditions on a high-brilliance Rigaku diffractometer (Mo Kα radiation) equipped with Osmic focusing X-ray optics and a Bruker Apex CCD detector. High-quality XRD measurements on bulk polycrystalline samples were carried out at ambient conditions on a STADI P (STOE) diffractometer in transmission geometry with a linear mini-PSD detector using Cu Kα_1 radiation (λ = 1.54056 Å) in the 2θ range from 5° to 120° with a step of 0.02°. Polycrystalline silicon [a = 5.43075(5)

dx.doi.org/10.1021/ic400649h | Inorg. Chem. 2013, 52, 11703−11710

Å] was used as an external standard for these XRD studies (Figures 3 and S7 in the SI). Single-crystalline samples (Figure 4) were

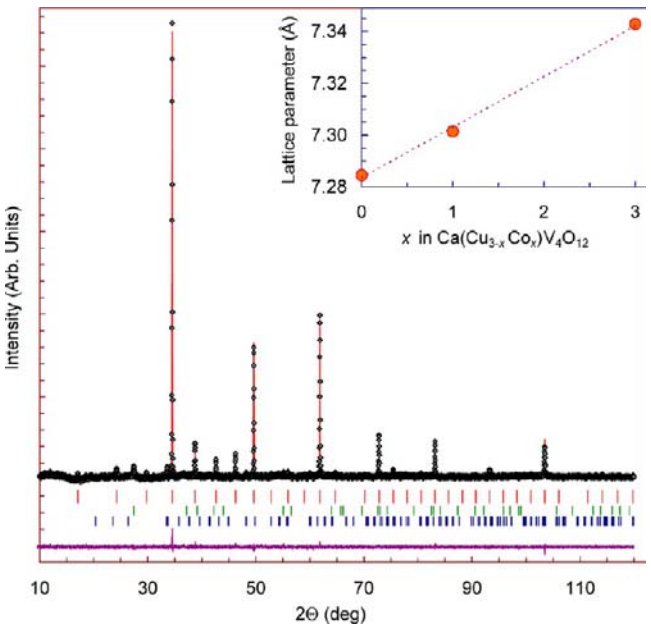

Figure 3. XRD pattern of $CaCo_3V_4O_{12}$ collected at ambient conditions. Points are experimental data, the solid line is the calculated profile, and the lowermost curve is the difference between the experimental and calculated profiles. The upper row of dashes denotes expected reflection positions for the $Im\bar{3}$ space group of $CaCo_3V_4O_{12}$; likewise, the middle row denotes expected reflection position for the $P4_2/mnm$ structure of VO_2, and the lower row denotes expected reflection position for the *Pnma* structure of $CaVO_3$. Inset: lattice parameters of $CaCo_3V_4O_{12}$ (this work), $CaCu_2CoV_4O_{12}$,[32] and $CaCu_3V_4O_{12}$.[16]

investigated at ambient conditions using a four-circle Oxford Diffraction Xcalibur diffractometer (λ = 0.71073 Å) equipped with an Xcalibur Sapphire2 CCD detector. Reflection intensities were measured by ω scanning of narrow (0.5°) frames. Data collection and further integration were performed with the assistance of *CrysAlis CCD*[35] and *CrysAlis RED*[36] software, respectively. Empirical absorption correction was applied using spherical harmonics, implemented in the *SCALE3 ABSPACK* scaling algorithm, which is included in the *CrysAlis RED* software. The structure of $CaCo_3V_4O_{12}$ (Figure 5) has been refined by full-matrix least squares in an anisotropic approximation for all atoms, using *SHELXL-97* and *SHELXTL* software.[37]

Magnetic susceptibility measurements (Figure 6) were carried out on a MPMS SQUID magnetometer in the temperature range 2−400 K in applied fields up to 5 T and on a VSM-5T vibrating-sample magnetometer (Cryogenic Ltd.) in a magnetic field of 1 T. Electronic transport properties (Figure 7) were measured by the conventional Montgomery method using an Oxford Instruments setup.[38,39]

In order to examine the thermal stability of $CaCo_3V_4O_{12}$ perovskite, we annealed several pieces of it in an oven for 10−20 min under air conditions at each temperature point starting at 230 °C. We found that oxidation and/or decomposition of $CaCo_3V_4O_{12}$ perovskite starts above 500 °C and is completed at 600 °C (Figure S13 in the SI).

RESULTS AND DISCUSSION

The black-colored samples of $CaCo_3V_4O_{12}$ showed good crystallinity and a wide dispersion of crystallite sizes (Figure 1a,b). The sample looked very uniform (Figure 1b,c). At HP-HT conditions, vanadium is known to be inclined to the formation of conventional perovskite phases (e.g., $PbVO_3$).[40] However, the conditions of our HP-HT synthesis were rather

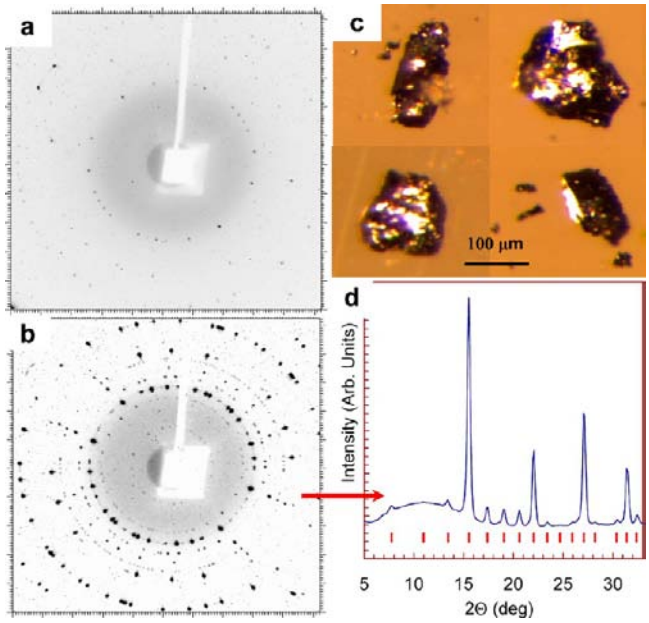

Figure 4. Typical XRD images (a and b), photographs (c), and a 2D integrated pattern (d; corresponding to the XRD image shown in part b) of twinned single crystals of $CaCo_3V_4O_{12}$. These XRD images have been collected on a Rigaku diffractometer under rotation of a sample around its axis over 360° during acquisition in order to form a ringlike XRD image. The dashes in the XRD pattern (d) indicate expected reflection positions for the $Im\bar{3}$ space group.

unfavorable for the formation of simple perovskites, such as the well-known $CaVO_3$[41] and others. A weight fraction of the $CaVO_3$ perovskite in our samples did not exceed ~3−4%.

The crystal structure of $CaCo_3V_4O_{12}$ was examined by XRD studies on bulk polycrystalline samples and small single crystals (Figures 3 and 4). The samples were also probed by SAED studies (Figures 1 and 2). The XRD pattern of a powder sample (Figures 3 and S7 in the SI) matches that of the $CaCu_3V_4O_{12}$ perovskite,[16] and hence we used the crystal structure data for the latter as a starting structural model for our perovskite. A full-profile Rietveld refinement of the XRD patterns (Figures 3 and S7 in the SI) confirmed this model. Thus, we found that $CaCo_3V_4O_{12}$ has a typical double-perovskite structure of $Im\bar{3}$ space group (No. 204) with a lattice parameter of a = 7.34285(5) Å (Figure 5). The refined atomic coordinates are summarized in Table 1. This $Im\bar{3}$ space group (No. 204) suggests only one crystallographic position for the V ions. The spot reflections in the SAED patterns collected at both 295 and 105 K (Figures 2 and S5 and S6 in the SI) unambiguously indicate a basic cubic symmetry corresponding to the above $Im\bar{3}$ space group. Notice that another common space group, $Pn\bar{3}$ (No. 201), which is possible in double perovskites showing charge disproportionation between the two B sites, would give an extra 111 reflection.[17] Our SAED studies did not detect such a reflection (Figure 2). One can notice that the lattice parameter of $CaCo_3V_4O_{12}$ and those found earlier in $CaCu_3V_4O_{12}$[16] and $Ca(Cu_{2/3}Co_{1/3})_3V_4O_{12}$[32] follow the linear Vegard's law (inset in Figure 3). Using a bond-valence-sum analysis,[42] we found $Ca^{2.2+}$, $Co^{1.9+}$, and $V^{4.1+}$ (see the SI for details). Then, the chemical formula of this perovskite can be written as follows: $Ca^{2+}Co_3^{2+}V_4^{4+}O_{12}$.

The XRD patterns collected on different samples cut from the $CaCo_3V_4O_{12}$ ingot also showed extra reflections that were assigned to $CaVO_3$ and VO_2 (Figure 3). A full-profile analysis

dx.doi.org/10.1021/ic400649h | Inorg. Chem. 2013, 52, 11703−11710

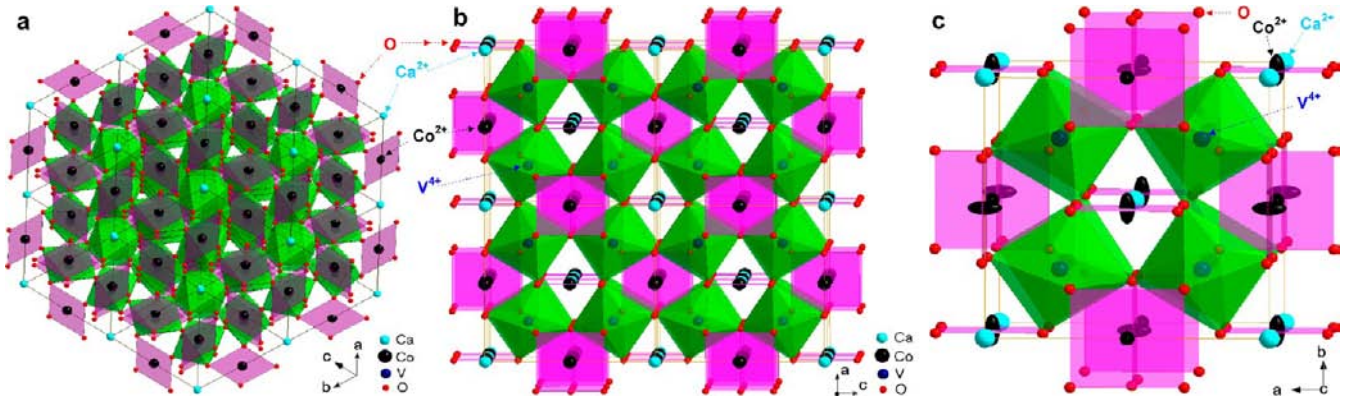

Figure 5. Double-perovskite crystal structure of $CaCo_3V_4O_{12}$. (a and b) Different views of 2 × 2 × 2 supercell blocks showing square-planar oxygen coordination of the Co^{2+} ions occupying the A′ sites and the octahedral network of the V^{4+} ions. (c) Anisotropic displacements of the Co^{2+} ions in the direction perpendicular to the plane of square-planar oxygen coordination found in single-crystal diffraction studies (Table 2). The solid lines are the unit cell boundaries.

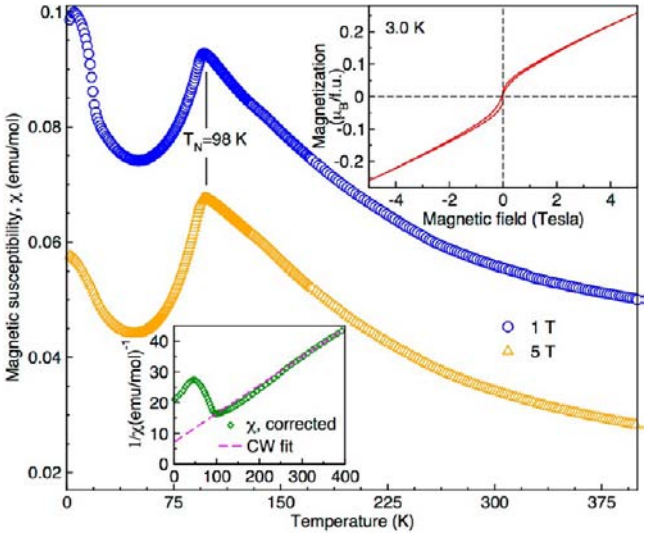

Figure 6. Magnetic susceptibility of $CaCo_3V_4O_{12}$ measured in the applied fields of 1 and 5 T. No difference between field-cooling and zero-field-cooling regimes was observed. Note the antiferromagnetic transition around 98 K and the field dependence related to a ferromagnetic impurity. The upper inset shows the field dependence of magnetization measured at 3 K. The lower inset presents the Curie–Weiss fit above 300 K for corrected susceptibility, as described in the text.

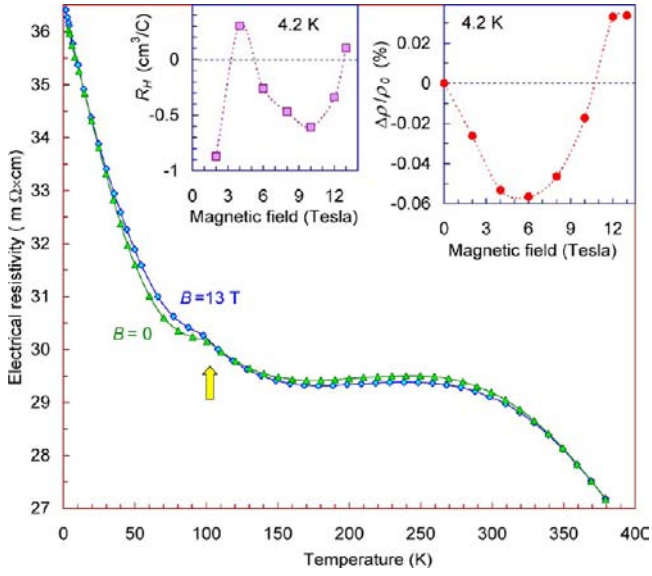

Figure 7. Temperature dependencies of the electrical resistivity of $CaCo_3V_4O_{12}$ at zero magnetic field and at 13 T. The bulk arrow indicates a steplike feature near 100 K. The two insets show dependencies of the magnetoresistance effect ($\Delta\rho/\rho_0$) and Hall constant (R_H) on the magnetic field at 4.2 K.

of the XRD pattern given in this paper (Figures 3 and S7 in the SI) yields the weight fractions of $CaVO_3$ and VO_2 as 3.0 and 4.6%, respectively.

Originally, the structural model of the $CaCo_3V_4O_{12}$ perovskite (Table 1) was determined from the powder XRD data (Figure 3). After a series of syntheses in variable HP-HT conditions, we eventually succeeded in the preparation of relatively big single crystals of $CaCo_3V_4O_{12}$ (Figure 4) and, hence, we performed single-crystal XRD studies on them. In preliminary XRD studies on the Rigaku diffractometer, we preselected several promising crystals (Figures 4 and S8 in the SI) and then examined them on an Oxford Diffraction Xcalibur diffractometer. Finally, the crystal structure was resolved on a bulk high-quality twinned crystal (Tables 2 and 3). The crystal structure models based on the powder (Table 1) and single-crystal XRD data (Table 2) are almost identical. Both show the strongest displacements of the Co^{2+} ions. The single-crystal XRD studies additionally provide the tensors of anisotropic displacements (U_{11}, U_{22}, U_{33}, U_{12}, U_{13}, and U_{23}). The displacements of the Ca^{2+} and V^{4+} ions are truly isotropic, and those of the oxygen atoms are also close to that (Table 2). In contrast, the Co^{2+} ions feature prolate thermal ellipsoids with large displacements in the direction perpendicular to the CoO_4 plane (Figure 5c). We did not observe any incommensurate reflections in these single-crystal XRD studies.

The presence of an array of dashlike reflections in the ambient and low-temperature SAED patterns (Figures 2 and S5 and S6 in the SI) hints that the lattice of this perovskite has signatures of incommensurate structural modulations (Figure 2a,c), and therefore the above structural model is an "average" structure. However, the strong smoothing of these reflections (Figure 2a,c) would suggest that atomic displacements related to these incommensurate modulations are ordered only at the short-range scale. In systems with well-defined incommensurate modulations, these extra reflections in SAED patterns would

dx.doi.org/10.1021/ic400649h | Inorg. Chem. 2013, 52, 11703–11710

Table 1. Unit Cell Parameters of $CaCo_3V_4O_{12}$ Found from Powder XRD Studies[a]

formula	$CaCo_3V_4O_{12}$
cryst syst, space group	cubic, $Im\bar{3}$ (No. 204)
$P-T$ conditions	ambient pressure, 298(2) K
lattice parameter (Å)	7.3428(6)
unit cell volume (Å^3)	395.91(1)
formula units in the cell, Z	2
calcd density (g cm^{-3})	5.14
radiation, wavelength (Å)	1.54056
diffractometer	STADI P (STOE)
2θ range (deg)	5−120
method of refinement	full profile
R_P and wR_P (%)	0.77, 0.98

		atomic coordinates			
atom	site	x/a	y/b	z/c	isotropic displacement U_{iso}[a] × 100, Å^2
Ca	2a	0	0	0	2.4(4)
Co	6b	0	0.5	0.5	4.7(4)
V	8c	0.25	0.25	0.25	3.0(2)
O	24g	0	0.2990(8)	0.8115(7)	2.7(1)

[a]These values correspond to the refinement shown in Figure S7 in the SI. A CIF file is given in the SI.

have shapes of spots.[43−46] Incommensurate structures generally show up in systems with competing periodicities.[47] They can also reflect the ordering of oxygen vacancies.[41,46,48,49] However, the full-profile Rietveld refinement of the XRD patterns of powder $CaCo_3V_4O_{12}$ (Figures 3 and S7 in the SI) and the refinement of the single-crystal XRD data reveal full occupation of all of the cation sites and exclude any appreciable anion deficiency. The incommensurate structural modulations seen on the SAED patterns (Figure 2a,c) should be rather ascribed to local displacements of the Co^{2+} ions out of the CoO_4 planes (Table 2 and Figures 5c and S9 in the SI). This could also explain the nonregular (short-range) character of these structural modulations (Figure 2a,c). More detailed SAED images are available in the SI (Figures S5 and S6).

Magnetic susceptibility (χ) measured on bulk polycrystalline samples of $CaCo_3V_4O_{12}$ shows a sharp maximum around 98 K (Figure 6), which is characteristic of an antiferromagnetic ordering transition. We performed magnetization measurements on three different samples with different amounts of impurity phases. All of the samples showed a 98 K transition together with several other features that changed from one sample to another. For example, the data shown in Figure 6 are field-dependent and, thus, indicative of a ferromagnetic contribution that persists up to at least 400 K [note also the weak hysteresis in the $M(H)$ curve shown as an inset of Figure 6]. Another sample lacked the ferromagnetic contribution at high temperatures but revealed a sizable ferromagnetic signal below 150 K (Figure S10 in the SI). Unfortunately, we cannot identify these ferromagnetic signals in terms of individual impurity phases. Both pure $CaVO_3$ and VO_2, which are seen in the XRD data (Figure 3), are not ferromagnetic. However, the presence of Co in the reaction mixture could produce doped versions of $CaVO_3$ and VO_2 that have not been studied so far. Nevertheless, the reproducibility of the 98 K transition in the three different samples proves its intrinsic nature, while the ferromagnetic contributions are certainly extrinsic (see also the SI). The presence of ferromagnetic impurities prevents us from detailed analysis of the low-field data, where ferromagnetic signals are prominent and conceal the intrinsic signal of $CaCo_3V_4O_{12}$.

The magnetization data were corrected for the ferromagnetic impurity signal as follows: $\chi_{corr} = M(5\ T) - M(1\ T)/(5\ T - 1\ T)$. The resulting χ_{corr} is the intrinsic signal of $CaCo_3V_4O_{12}$. It follows the linear regime in $1/\chi$ above 200 K, with a slight change in the slope around 300 K (Figure 6). Above 300 K, we

Table 2. Unit Cell Parameters of $CaCo_3V_4O_{12}$ Found in Single-Crystal XRD Studies[a]

formula	$CaCo_3V_4O_{12}$
cryst syst, space group	cubic, $Im\bar{3}$ (No. 204)
$P-T$ conditions	ambient pressure, 293(2) K
lattice parameter (Å)	7.3429(10)
unit cell volume (Å^3)	395.92(1)
formula units in the cell, Z	2
calcd density (g cm^{-3})	5.14
radiation, wavelength (Å)	0.71073
diffractometer	Oxford Diffraction Xcalibur
abs coeff (mm^{-1})	11.371
$F(000)$	289
θ range for data collection (deg)	3.92−32.02
index ranges	$-10 \le h \le 10$, $-10 \le k \le 10$, $-10 \le l \le 6$
reflns collected	135
method of refinement	full-matrix least squares on F^2
GOF on F^2	1.167
R_P and wR_P (%)	3.75, 10.94

		atomic coordinates			anisotropic displacements,[b] U^a × 100, Å^2		
atom	site	x/a	y/b	z/c	U_{11}	U_{22}	U_{33}
Ca	2a	0	0	0	0.95(7)	0.95(7)	0.95(7)
Co	6b	0	0.5	0.5	0.83(7)	0.91(7)	4.32(10)
V	8c	0.25	0.25	0.25	0.67(5)	0.67(5)	0.67(5)
O	24g	0	0.2992(4)	0.8115(4)	0.96(14)	1.22(17)	1.07(19)

[a]A CIF file is supplied. [b]U_{12}, U_{13}, and U_{23} were negligibly small.

dx.doi.org/10.1021/ic400649h | Inorg. Chem. 2013, 52, 11703−11710

Table 3. Main Distances and Angles in the Perovskite Structure of $CaCo_3V_4O_{12}$ in the Structural Model Given in Table 2

distance (Å)			some bond angles (deg)			
Ca−O	12×	2.596(7)	O−Ca−O	116.81(3)	Ca−O−Co	104.60(1)
Co−O	4×	2.022(3)	O−Ca−O	63.19(3)	Co−O−V	107.30(9)
Co−O	4×	2.721(4)	O−Ca−O	64.42(1)	V−O−V	145.03(2)
Co−O	4×	3.171(5)	O−Co−O	86.37(2)	Ca−O−V	88.07(9)
V−O	6×	1.924(7)	O−Co−O	93.63(2)		
Ca−V	8×	3.179(6)	O−V−O	89.95(1)		
Co−V	8×	3.179(6)				

found C = 10.86 emu K^{-1} mol^{-1} and Θ = −79 K according to the Curie−Weiss fit with $\chi = C/(T - \Theta)$. The Curie constant C yields an effective moment (μ_{eff}) of about 9.3 μ_B/fu, whereas the negative Θ conforms to the antiferromagnetic nature of the 98 K transition. The change in the slope around 300 K is probably extrinsic because it has not been seen in another sample of $CaCo_3V_4O_{12}$ (see Figure S12 in the SI).

Electrical resistivity measured on a bulk polycrystalline sample of $CaCo_3V_4O_{12}$ demonstrates semimetal behavior with a steplike anomaly around 100 K (Figure 7). This anomaly has a direct correspondence with the antiferromagnetic ordering transition shown in Figure 6. The resistivity curve looks similar to those reported for some other perovskites, e.g., for $CaCu_3Fe_4O_{12}$.[17] Near ambient conditions, we observed negative values of the Hall effect (R_H) in $CaCo_3V_4O_{12}$, indicating a dominating n-type conductivity. We found that the carrier concentration and mobility are approximately $n \sim (1-3) \times 10^{19}$ cm^{-3} and $\mu \sim 5-25$ cm^2 V^{-1} s^{-1} within the temperature range investigated. Magnetic-field dependencies of the Hall and magnetoresistance effect obtained at 4.2 K (insets in Figure 7) suggest that the low-temperature state of $CaCo_3V_4O_{12}$ is very sensitive to the magnetic field. A negative magnetoresistance effect found under the application of moderate magnetic fields was observed also in $CaCu_3Fe_4O_{12}$.[17] Additionally, we observed a nonmonotonic change in the resistivity around 300 K, which is reminiscent of the change in the slope of $1/\chi_{corr}$ around the same temperature. However, the origin of this effect is presently unclear and requires further investigation.

In the simplest picture, delocalization of the B-cation d electrons is determined by the bandwidth, which, in turn, depends on the V−O−V angles that are reduced by the strong tilting distortion in the $AA'_3B_4O_{12}$ double perovskites. The V−O−V angle of 145.03(2)° in $CaCo_3V_4O_{12}$ (Table 3) is close, for instance, to that of 145.4(2)° in the $CaCu_3V_4O_{12}$ perovskite,[16] which shows metallic behavior.[26,50] On the other hand, our resistivity data evidence nonmetallic behavior. Therefore, in analysis of the effective paramagnetic moment derived from the susceptibility data (Figure 6), we considered two limiting cases of the fully itinerant and fully localized V^{4+} electrons. The case of the itinerant V^{4+} electrons implies that the effective paramagnetic moment derived from the susceptibility data should be solely ascribed to the Co^{2+} ions, and in this way, we obtain $\mu_{eff} \sim 5.4$ μ_B/Co. In the case of completely localized V^{4+} electrons, we also account for the effective moment of 1.73 μ_B on each of the spin $^1/_2$ V^{4+} ions and obtain $\mu_{eff} \sim 5.0$ μ_B/Co (note that χ is proportional to μ_{eff}^2). Both of these values are well above the spin-only magnetic moment expected for the high-spin (HS) Co^{2+}, with its electronic configuration $3t_{2g}^5e_g^2$ yielding $\mu_{eff} \sim 3.87$ μ_B for a spin $^3/_2$ ion. The low-spin (LS) Co^{2+} with the electronic configuration $3t_{2g}^6e_g^1$ would have a much lower effective moment of 1.73 μ_B. Therefore, in $CaCo_3V_4O_{12}$, the magnetic moment of Co^{2+} is strongly enhanced compared to its spin-only value.

The departure of the effective magnetic moment from its spin-only value is most likely related to the orbital moment, which is very typical for Co^{2+}.[51−54] Our data suggest an orbital moment exceeding 1 μ_B, in agreement with earlier studies of Co^{2+} oxides.[51−54] However, formation of the orbital moment intimately depends on the crystal-field levels and details of the local environment. Because $CaCo_3V_4O_{12}$ features an unprecedented square-planar coordination of Co^{2+} (Figures 5c and S9 in the SI), formation of the large orbital moment may not follow the existing theoretical framework and clearly deserves further investigation.

The magnetic structure of $CaCo_3V_4O_{12}$ could be further investigated by neutron diffraction, which probes the magnetic moment on the Co site and, thus, provides a direct estimate of the orbital component. Neutron diffraction studies have been instrumental in understanding the complex crystal and magnetic structures of ambient and high-pressure layered perovskite polymorphs of $La_4Cu_3MoO_{12}$.[55−58] Additionally, magnetic transitions are often coupled with remarkable structural transformations[9,17,59,60] that may be present in $CaCo_3V_4O_{12}$ as well.

The formation of the double-perovskite structures at HP-HT conditions depends on several factors, including the competition between different versions of the perovskite structure and the capability of transition-metal cations to adopt the square-planar local environment via Jahn−Teller distortion. A Jahn−Teller effect is expected to be strong if the e_g orbitals are filled by odd numbers of electrons.[19] This is the case in the Cu^{2+} ions (electron configuration Ar $3d^9 = 3t_{2g}^6e_g^3$) and in the Mn^{3+} ions alike (Ar $3d^4 = 3t_{2g}^3e_g^1$ in the HS state).[19] The Jahn−Teller effect explains the existence of multiple perovskites in which the A′ sites having square-planar oxygen coordination are filled either by the Cu^{2+} ions or by the HS Mn^{3+} ones.[9−18,21−25] The Co^{2+} ions are also Jahn−Teller active in both the LS ($3t_{2g}^6e_g^1$) and HS ($3t_{2g}^5e_g^2$) states. However, they are less likely to show strong Jahn−Teller distortions because the orbital degeneracy may be lifted through a different mechanism, stabilization of a multiplet with the large orbital moment via an energy gain from the reduced Coulomb repulsion.[52,61] Our observation of the large orbital moment is reminiscent of this scenario, although the square-planar local environment of Co^{2+} implies that Jahn−Teller distortion is present as well and probably plays a role in lifting the orbital degeneracy.

One should recall that the $CaCo_3V_4O_{12}$ perovskite is a high-pressure polymorph that cannot be synthesized at ambient-pressure conditions. It is plausible that the formation of this polymorph requires the transformation of Co^{2+} ions to the LS state, which is more suitable for the square-planar oxygen environment in this double-perovskite structure. Upon the release of pressure, Co^{2+} ions should return to the HS state

dx.doi.org/10.1021/ic400649h | Inorg. Chem. 2013, 52, 11703−11710

with a concurrent and significant increase in the ionic radius. This might explain the abnormally strong displacements of the Co^{2+} ions out of the CoO_4 plane (Table 2 and Figure 5c). Probably, the electronic orbitals in these "grasped" HS Co^{2+} ions are also "deformed" in comparison with the ordinary HS Co^{2+} cases in other materials. Note that pressure-induced spin-state transitions are rather common for cobalt oxides, such as, e.g., in $BiCoO_3$.[62]

Altogether, we have shown that the robust square-planar local environment is not a necessary requirement for the formation of $AA'_3B_4O_{12}$ double-perovskite structures. Our results are in line with other recent studies showing variable transition-metal cations occupying the A′ sites, e.g., $Na(Cu_{2.5}Ti^{4+}_{0.5})Ti_4O_{12}$,[20] $Sr_{0.946}(Cu_{2.946}Ti_{0.054})Ti_4O_{12}$,[63] $NaMn^{2.33+}{}_3V_4O_{12}$,[27] and $(Ca,La)Mn^{2+}{}_3V_4O_{12}$.[27] Thus, HP-HT synthesis of a cubic $CaCo_3V_4O_{12}$ perovskite not only establishes a new class of $ACo_3B_4O_{12}$ double perovskites but also suggests a new intriguing trend in perovskite science and technology. We believe that even transition-metal ions with only weak Jahn–Teller distortions (e.g., Fe^{2+}, Fe^{3+}, Ti^{3+}, and V^{3+}) or without Jahn–Teller distortions at all are potential candidates for occupying the A′ sites in double-perovskite structures.

CONCLUSION

In this work, we have synthesized the first double perovskite with Co^{2+} ions at the A′ sites, $CaCo_3V_4O_{12}$. We have determined the oxidations states of the Co and V ions as 2+ and 4+, respectively, and established the HS state of Co^{3+} with a large orbital moment. This case is opposite to the overwhelming majority of double perovskites in which the A′ sites are occupied by ions having strong Jahn–Teller distortion, namely, Cu^{2+} and HS Mn^{3+}.[9−18,21−25] Considering other recent examples of the $AA'_3B_4O_{12}$ perovskites with non-Jahn–Teller-active A′ cations (e.g., Ti^{4+}, Mn^{2+}, Fe^{2+}),[20,27,29] we suggest that a much larger family of the $AA'_3B_4O_{12}$ compounds may exist and show unique electronic properties.

$CaCo_3V_4O_{12}$ orders antiferromagnetically around 100 K. The low-temperature phase of $CaCo_3V_4O_{12}$ and its crystal and magnetic structures require further investigation. The magnetic behavior of $CaCo_3V_4O_{12}$ is different from that of other double perovskites; e.g., $CaCu_3V_4O_{12}$ is paramagnetic,[8,16] and iron-containing perovskites, like $ACu_3Fe_4O_{12}$, demonstrate a ferromagnetic ordering transition upon cooling.[9,11,17,18] Synthesis of $CaCo_3V_4O_{12}$ reveals the existence of a new class of double perovskites, $ACo_3B_4O_{12}$, in which the A sublattice may be occupied by lanthanides, sodium, strontium, and bismuth and by other elements and the B sublattice by some transition metals.

ASSOCIATED CONTENT

Supporting Information

Detailed information of the crystal structure (CIF files), XRD and electron diffraction patterns, EDX spectra, TEM and SEM images, and data on magnetic properties. This material is available free of charge via the Internet at http://pubs.acs.org.

AUTHOR INFORMATION

Corresponding Author

*E-mail: sergey.ovsyannikov@uni-bayreuth.de or sergey2503@gmail.com.

Notes

The authors declare no competing financial interest.

ACKNOWLEDGMENTS

The authors are grateful to Dr. S. Shcheka for useful comments and assistance in the microprobe characterization of the samples and Drs. D. M. Trots and T. Boffa Ballaran for assistance in the single-crystal XRD studies and data analysis. The authors are grateful to three anonymous reviewers for careful reading of the manuscript and useful advice on its improvement. S.V.O. thanks the Deutsche Forschungsgemeinschaft (DFG; Grants OV 110/1-1 and OV 110/1-2) Foundation for financial support. A.A.T. acknowledges financial support from the ESF through the Motilitas program (Grant MTT77).

REFERENCES

(1) Tejuca, L. G. *Properties and applications of perovskite-type oxides*; Dekker: New York, 1993.
(2) Mitchell, R. H. *Perovskites: modern and ancient*; Almaz Press: Thunder Bay, Ontario, Canada, 2002.
(3) King, G.; Woodward, P. M. *J. Mater. Chem.* **2010**, *20*, 5785–5796.
(4) Vasil'ev, A. N.; Volkova, O. S. *Low-Temp. Phys.* **2007**, *33*, 895–914.
(5) Longo, J.; Ward, R. *J. Am. Chem. Soc.* **1961**, *83*, 2816–2818.
(6) Anderson, M. T.; Greenwood, K. B.; Taylor, G. A.; Poeppelmeier, K. R. *Prog. Solid State Chem.* **1993**, *22*, 197–233.
(7) Kabayashi, K.-I.; Kimura, T.; Sawada, H.; Terakura, K.; Tokura, Y. *Nature* **1998**, *395*, 677–680.
(8) Shimakawa, Y. *Inorg. Chem.* **2008**, *47*, 8562–8570.
(9) Long, Y. W.; Hayashi, N.; Saito, T.; Azuma, M.; Muranaka, S.; Shimakawa, Y. *Nature* **2009**, *458*, 60–63.
(10) Long, Y.-W.; Kawakami, T.; Chen, W.-T.; Saito, T.; Watanuki, T.; Nakakura, Y.; Liu, Q.-Q.; Jin, C.-Q.; Shimakawa, Y. *Chem. Mater.* **2012**, *24*, 2235–2239.
(11) Chen, W.-T.; Saito, T.; Hayashi, N.; Takano, M.; Shimakawa, Y. *Sci. Rep.* **2012**, *2*, 449.
(12) Subramanian, M. A.; Li, D.; Duan, N.; Reisner, B. A.; Sleight, A. W. *J. Solid State Chem.* **2000**, *151*, 323–325.
(13) Homes, C. C.; Vogt, T.; Shapiro, S. M.; Wakimoto, S.; Ramirez, A. P. *Science* **2001**, *27*, 673–676.
(14) Zeng, Z.; Greenblatt, M.; Subramanian, M. A.; Croft, M. *Phys. Rev. Lett.* **1999**, *82*, 3164–3167.
(15) Kobayashi, W.; Terasaki, I.; Takeya, J.; Tsukada, I.; Ando, Y. *J. Phys. Soc. Jpn.* **2004**, *73*, 2373–2376.
(16) Kadyrova, N. I.; Tyutyunnik, A. P.; Zubkov, V. G.; Zakharova, G. S.; Volkov, V. L.; Dyachkova, T. V.; Zainulin, Yu. G. *Russ. J. Inorg. Chem.* **2003**, *48*, 776–778.
(17) Yamada, I.; Takata, K.; Hayashi, N.; Shinohara, S.; Azuma, M.; Mori, S.; Muranaka, S.; Shimakawa, Y.; Takano, M. *Angew. Chem., Int. Ed.* **2008**, *47*, 7032–7035.
(18) Yamada, I.; Takahashi, Y.; Ohgushi, K.; Nishiyama, N.; Takahashi, R.; Wada, K.; Kunimoto, T.; Ohfuji, H.; Kojima, Y.; Inoue, T.; Irifune, T. *Inorg. Chem.* **2010**, *49*, 6778–6780.
(19) Pavarini, E. Crystal-Field Theory, Tight-Binding Method and Jahn–Teller Effect. In *Correlated Electrons: From Models to Materials*; Pavarini, E., Koch, E., Anders, F., Jarrell, M., Eds.; July 2012, http://en.wikipedia.org/wiki/Jahn%E2%80%93Teller_effect.
(20) Avdeev, M.; Nalbandyan, V. B. *Inorg. Chem.* **2006**, *45*, 2217–2220.
(21) Prodi, A.; Gilioli, E.; Gauzzi, A.; Licci, F.; Marezio, M.; Bolzoni, F.; Huang, Q.; Santoro, A.; Lynn, J. W. *Nat. Mater.* **2004**, *3*, 48–52.
(22) Cabassi, R.; Bolzoni, F.; Gilioli, E.; Bissoli, F.; Prodi, A.; Gauzzi, A. *Phys. Rev. B* **2010**, *81*, 214412.
(23) Imamura, N.; Karppinen, M.; Yamauchi, H. *Chem. Mater.* **2009**, *21*, 2179–2183.
(24) Gauzzi, A.; Rousse, G.; Mezzadri, F.; Calestani, G. L.; Andre, G.; Bouree, F.; Calicchio, M.; Gilioli, E.; Cabassi, R.; Bolzoni, F.; Prodi, A.; Bordet, P.; Marezio, M. *J. Appl. Phys.* **2013**, *113*, 043920.

(25) Locherer, T.; Dinnebier, R.; Kremer, R. K.; Greenblatt, M.; Jansen, M. *J. Solid State Chem.* **2012**, *190*, 277−284.
(26) Shikari, H.; Saito, T.; Azuma, M.; Shimakawa, Y. *J. Phys. Soc. Jpn.* **2008**, *77*, 064705.
(27) Zhang, S.; Saito, T.; Mizumaki, M.; Chen, W. T.; Tohyama, T.; Shimakawa, Y. *J. Am. Chem. Soc.* **2012**, *135*, 6056−6060.
(28) Shiro, K.; Yamada, I.; Ikeda, N.; Ohgushi, K.; Mizumaki, M.; Takahashi, R.; Nishiyama, N.; Inoue, T.; Irifune, T. *Inorg. Chem.* **2013**, *52*, 1604−1609.
(29) Leinenweber, K.; Linton, J.; Navrotsky, A.; Fei, Y.; Parise, J. B. *Phys. Chem. Miner.* **1995**, *22*, 251−258.
(30) Ovsyannikov, S. V.; Abakumov, A. M.; Tsirlin, A. A.; Schnelle, W.; Egoavil, R.; Verbeeck, J.; Van Tendeloo, G.; Glazyrin, K.; Hanfland, M.; Dubrovinsky, L. *Angew. Chem., Int. Ed.* **2013**, *52*, 1494−1498.
(31) Kadyrova, N. I.; Zainulin, Yu. G.; Tyutyunnik, A. P.; Mel'nikova, N. V.; Ustinova, I. S. *Inorg. Mater.* **2011**, *47*, 1396−1401.
(32) Kadyrova, N. I.; Zainulin, Yu. G.; Zakharova, G. S.; Tyutyunnik, A. P.; Mel'nikova, N. V. *Russ. J. Inorg. Chem.* **2011**, *56*, 1715−1720.
(33) Frost, D. J.; Poe, D. N.; Tronnes, R. G.; Liebske, C.; Duba, A.; Rubie, D. C. *Phys. Earth Planet. Inter.* **2004**, *143*−*144*, 507−514.
(34) Ovsyannikov, S. V.; Dubrovinsky, L. *High Press. Res.* **2011**, *31*, 23−29.
(35) *CrysAlis CCD*; Oxford Diffraction Ltd.: Abingdon, England, 2006.
(36) *CrysAlis RED*; Oxford Diffraction Ltd.: Abingdon, England, 2006.
(37) Sheldrick, G. M. *SHELXL97*; University of Göttingen: Göttingen, Germany, 1997.
(38) Karkin, A. E.; Yangirov, M. R.; Akshentsev, Yu. N.; Goshchitskii, B. N. *Phys. Rev. B* **2011**, *84*, 054541.
(39) Ovsyannikov, S. V.; Wu, X.; Karkin, A. E.; Shchennikov, V. V.; Manthilake, G. M. *Phys. Rev. B* **2012**, *86*, 024106.
(40) Shpanchenko, R. V.; Chernaya, V. V.; Tsirlin, A. A.; Chizhov, P. S.; Sklovsky, D. E.; Antipov, E. V.; Khlybov, E. P.; Pomjakushin, V.; Balagurov, A. M.; Medvedeva, J. E.; Kaul, E. E.; Geibel, C. *Chem. Mater.* **2004**, *16*, 3267−3273.
(41) Ueda, Y.; Nakayama, N. *Solid State Ionics* **1998**, *108*, 303−306.
(42) Brese, N. E.; O'Keffee, M. *Acta Crystallogr.* **1991**, *B47*, 192−197.
(43) Rusakov, D. A.; Abakumov, A. M.; Yamaura, K.; Belik, A. A.; Van Tendeloo, G.; Takayama-Muromachi, E. *Chem. Mater.* **2011**, *23*, 285−292.
(44) García-Martín, S.; King, G.; Urones-Garrote, E.; Nénert, G.; Woodward, P. M. *Chem. Mater.* **2011**, *23*, 163−170.
(45) García-Martín, S.; King, G.; Nénert, G.; Ritter, C.; Woodward, P. M. *Inorg. Chem.* **2012**, *51*, 4007−4014.
(46) Dachraoui, W.; Hadermann, J.; Abakumov, A. M.; Tsirlin, A. A.; Batuk, D.; Glazyrin, K.; McCammon, C.; Dubrovinsky, L.; Van Tendeloo, G. *Chem. Mater.* **2012**, *24*, 1378−1385.
(47) Bak, P. *Rep. Prog. Phys.* **1982**, *45*, 587−629.
(48) Abakumov, A. M.; Batuk, D.; Hadermann, J.; Rozova, M. G.; Sheptyakov, D. V.; Tsirlin, A. A.; Niermann, D.; Waschkowski, F.; Hemberger, J.; Van Tendeloo, G.; Antipov, E. V. *Chem. Mater.* **2011**, *23*, 255−265.
(49) Van Tendeloo, G.; Hadermann, J.; Abakumov, A. M.; Antipov, E. V. *J. Mater. Chem.* **2009**, *19*, 2660−2670.
(50) Xiang, H.; Wu, Z. *Inorg. Chem.* **2008**, *47*, 2706−2709.
(51) Burnus, T.; Hu, Z.; Haverkort, M. W.; Cezar, J. C.; Flahaut, D.; Hardy, V.; Maignan, A.; Brookes, N. B.; Tanaka, A.; Hsieh, H. H.; Lin, H.-J.; Chen, C. T.; Tjeng, L. H. *Phys. Rev. B* **2006**, *74*, 245111.
(52) Burnus, T.; Hu, Z.; Wu, H.; Cezar, J. C.; Niitaka, S.; Takagi, H.; Chang, C. F.; Brookes, N. B.; Lin, H.-J.; Yang, L. Y.; Tanaka, A.; Liang, K. S.; Chen, C. T.; Tjeng, L. H. *Phys. Rev. B* **2008**, *77*, 205111.
(53) Lenertz, M.; Alaria, J.; Stoeffler, D.; Colis, S.; Dinia, A.; Mentré, O.; André, G.; Porcher, F.; Suard, E. *Phys. Rev. B* **2012**, *86*, 214428.
(54) Markkula, M.; Arévalo-López, A.; Attfield, J. P. *Phys. Rev. B* **2012**, *86*, 134401.
(55) Vander Griend, D. A.; Boudin, S.; Poeppelmeier, K. R.; Azuma, M.; Toganoh, H.; Takano, M. *J. Am. Chem. Soc.* **1998**, *120*, 11518−11519.
(56) Vander Griend, D. A.; Boudin, S.; Caignaert, V.; Poeppelmeier, K. R.; Wang, Y. G.; Dravid, V. P.; Azuma, M.; Takano, M.; Hu, Z. B.; Jorgensen, J. D. *J. Am. Chem. Soc.* **1999**, *121*, 4787−4792.
(57) Azuma, M.; Odaka, T.; Takano, M.; Vander Griend, D. A.; Poeppelmeier, K. R.; Narumi, Y.; Kindo, K.; Mizuno, Y.; Maekawa, S. *Phys. Rev. B* **2000**, *62*, R3588−R3591.
(58) Enterkin, J. A.; Maggard, P. A.; Ishiwata, S.; Marks, L. D.; Poeppelmeier, K. R.; Azuma, M.; Takano, M. *J. Solid State Chem.* **2010**, *183*, 551−556.
(59) Khalifah, P.; Osborn, R.; Huang, Q.; Zandbergen, H. W.; Jin, R.; Liu, Y.; Mandrus, D.; Cava, R. J. *Science* **2002**, *297*, 2237−2240.
(60) Tomioka, Y.; Okuda, T.; Okimoto, Y.; Asamitsu, A.; Kuwahara, H.; Tokura, Y. *J. Alloys Compd.* **2001**, *326*, 27−35.
(61) Wu, H.; Hu, Z.; Khomskii, D. I.; Tjeng, L. H. *Phys. Rev. B* **2007**, *75*, 245118.
(62) Oka, K.; Azuma, M.; Chen, W.; Yusa, H.; Belik, A. A.; Takayama-Muromachi, E.; Mizumaki, M.; Ishimatsu, N.; Hiraoka, N.; Tsujimoto, M.; Tucker, M. G.; Attfield, J. P.; Shimakawa, Y. *J. Am. Chem. Soc.* **2010**, *132*, 9438−9443.
(63) Li, J.; Subramanian, M. A.; Rosenfeld, H. D.; Jones, C. Y.; Toby, B. H.; Sleight, A. W. *Chem. Mater.* **2004**, *16*, 5223−5225.